Supporting Information

Tailoring the Linking Patterns of Polypyrene Cathodes for High-Performance Aqueous Zn Dual-Ion Batteries

Chong Zhang,[a] Wenyan Ma,[a] Changzhi Han,[a] Lian-Wei Luo,[a] Aigerim Daniyar,[b] Sihui Xiang,[a] Xianyong Wu,[b] Xiulei Ji*,[b] and Jia-Xing Jiang*,[a]

[a]Key Laboratory of Applied Surface and Colloid Chemistry (Shaanxi Normal University), Ministry of Education, Key Laboratory for Macromolecular Science of Shaanxi Province, Shaanxi Key Laboratory for Advanced Energy Devices, School of Materials Science and Engineering, Shaanxi Normal University, Xi'an 710062, P. R. China.
E-mail: jiaxing@snnu.edu.cn

[b]Department of Chemistry, Oregon State University, Corvallis, OR, 97331-4003, United States.
E-mail: david.ji@oregonstate.edu

Experimental section

***Materials**:*

Pyrene, 1,5-cyclooctadiene (cod), bis(1,5-cyclooctadine)nickel ($Ni(cod)_2$), bis(1,5-cyclooctadiene)dimethoxydiiridium, 2,2′-bipyridyl,N,N-dimethylformamide (DMF), tetrahydrofuran, N-methyl pyrrolidone (NMP), $CuBr_2$, $ZnCl_2$, and Zinc foil (0.1 mm thick) were purchased from Acros, Alfa, TCI, and Aldrich, and they were used as received. Hexane, ethyl acetate, dichloromethane, methanol, ethanol and acetone were purchased from Sinopharm. Glass fiber (GF/D borosilicate) was purchased from Whatman. Carbon paper was purchased from Fuel Cell Store. The compounds of 1,3,6,8-tetrabromopyrene, 2,7-dibromopyrene, 1,3,6,8-tetrakis(4,4,5,5-tetramethyl-1,3,2-dioxaborolan-2-yl)pyrene and 1,6-dibromopyrene were prepared according to the literatures.[1-4]

***Methods**:*

*Synthesis of **LPy-1***: Under the protection of N_2, 1,5-cyclooctadiene (1.01 mL, 8 mmol) was added into the solution of bis(1,5-cyclooctadine)nickel (2.15 g, 7.8 mmol) and 2,2′-bipyridyl (1.22 g, 7.8 mmol) in 150 mL DMF. The mixture was stirred at 80 °C for 1 hour to form the catalyst system. Then the solution of 2,7-dibromopyrene (500 mg, 1.4 mmol) in 40 mL DMF was added to the above solution and the resulting mixture was stirred at 80 °C for another 24 hours. After cooling to room temperature, to the mixture concentrated HCl (50 mL) was added. The precipitate was collected by filtrating and washed by methanol and water. LPy-1 was dried in vacuum oven at 90 °C and obtained with a yield of 72.7 %.

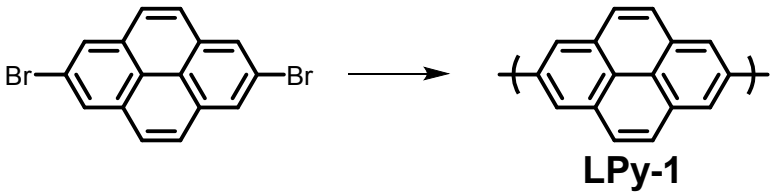

LPy-1

*Synthesis of **LPy-2***: Under the protection of N_2, 1,5-cyclooctadiene (1.01 mL, 8 mmol) was added

into the solution of bis(1,5-cyclooctadine)nickel (2.15 g, 7.8 mmol) and 2,2′-bipyridyl (1.22 g, 7.8 mmol) in 80 mL DMF. The mixture was stirred at 80 °C for 1 hour to form the catalyst system. Then the solution of 1,6-dibromopyrene (500 mg, 1.4 mmol) in 40 mL DMF was added to the above solution and the resulting mixture was stirred at 80 °C for another 24 hours. After cooling to room temperature, to the mixture concentrated HCl (50 mL) was added. The precipitate was collected by filtrating and washed by methanol and water. LPy-2 was dried in vacuum oven at 90 °C and obtained with a yield of 61.4 %.

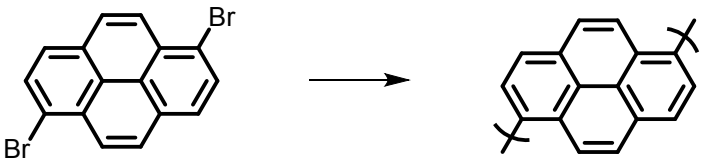

LPy-2

Synthesis of ***CLPy***: Under the protection of N_2, 1,5-cyclooctadiene (1.01 mL, 8 mmol) was added into the solution of bis(1,5-cyclooctadine)nickel (2.15 g, 7.8 mmol) and 2,2′-bipyridyl (1.22 g, 7.8 mmol) in 150 mL DMF. The mixture was stirred at 80 °C for 1 hour to form the catalyst system. Then 1,3,6,8-tetrabromopyrene (771 mg, 1.5 mmol) was added to the above solution and the resulting mixture was stirred at 80 °C for another 24 hours. After cooling to room temperature, to the mixture concentrated HCl (50 mL) was added. The precipitate was collected by filtrating and washed by methanol, water, acetone, and dichloromethane. CLPy was dried in vacuum oven at 90 °C and obtained with a yield of 76.1 %.

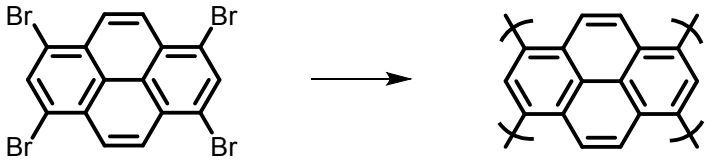

CLPy

Synthesis of ***CL12Py***: The chemicals of tetrakis(triphenylphosphine)palladium (0) (15 mg, 0.01 mmol), K_2CO_3 (1.1 g , 8.0 mmol), 2,7-dibromopyrene (720 mg, 2 mmol), and 1,3,6,8-

tetrakis(4,4,5,5-tetramethyl-1,3,2-dioxaborolan-2-yl)pyrene (706 mg, 1 mmol), were added into a 100 mL round bottom flask. The solvents of DMF (20 mL) and water (4 mL) were injected into the above flask in order. The reaction mixture was stirred at 150 °C for 48 h. After cooling down to temperature, the resulting precipitate was collected by filtration and thoroughly washed with methanol, H_2O, acetone and CH_2Cl_2. The product was collected and dried in vacuum at 90 °C for 24 h (yield, 75.5%).

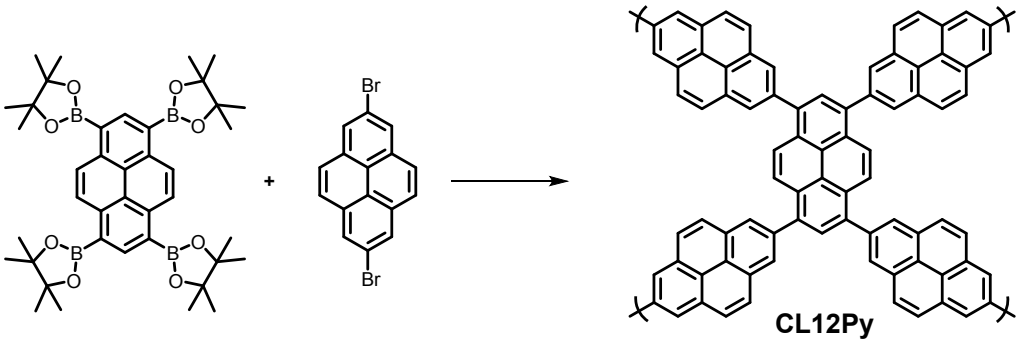

Synthesis of ***CL16Py***: The chemicals of tetrakis(triphenylphosphine)palladium (0) (15 mg, 0.01 mmol), 1,3,6,8-tetrakis(4,4,5,5-tetramethyl-1,3,2-dioxaborolan-2-yl)pyrene (706 mg, 1 mmol), K_2CO_3 (1.1 g , 8.0 mmol), and 1,6-dibromopyrene (720 mg, 2 mmol) were added into a 100 mL round bottom flask. The solvents of DMF (10 mL) and water (4 mL) were injected into the above flask in order. The reaction mixture was stirred at 150 °C for 72 h. After cooling down to temperature, the resulting precipitate was collected by filtration and thoroughly washed with methanol, H_2O, acetone and CH_2Cl_2. The product was collected and dried in vacuum at 90 °C for 24 h (yield, 61.4%).

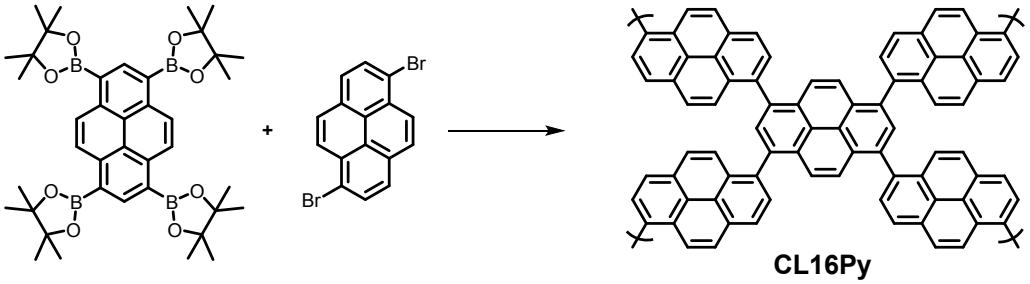

Materials characterization and method: Solid-state ^{1}H-^{13}C CP/MAS NMR measurements were conducted on a JEOL RESONRNCE ECZ 400R NMR spectrometer at a MAS rate of 12 kHz. FTIR spectra were carried out on a NICOLET 5397 AVATAR 360 FTIR. PXRD was recorded on a DX-2700B diffractometer with Cu Kα radiation. Thermogravimetric analysis (TGA) measurement was performed by using a differential thermal analysis instrument (Q1000DSC + LNCS + FACS Q600SDT) over the temperature range from 25 to 800 ^{o}C under a nitrogen atmosphere with a heating rate of 10 $^{o}Cmin^{-1}$. The elemental analysis measurement was achieved on a EURO EA30000 Elemental Analyzer. The morphology and element analysis of polypyrenes were collected on an environmental scanning electron microscopy with an energy dispersive spectrometer (FEI QUANTA 600F). The specific surface area and pore size distributions was evaluated by N_2 adsorption at 77 K on an ASAP 2420-4 (Micromeritics) volumetric adsorption analyzer. Surface area was calculated in the relative pressure (P/P_0) ranging from 0.05 to 0.20. Sample was degassed at 120 °C for 12 h under vacuum (10^{-5} bar) before analysis. Electron paramagnetic resonance measurement was conducted on the E500 (Bruker) to monitor the strength of pyrene radicals at different states. The DFT simulation on the electronic structure of polypyrenes was conducted by using Gaussian 09 at the B3LYP/6-31g(d) level. Density functional theory calculations for the binding energy are performed with the projector augmented wave (PAW) method. The exchange-functional is treated using the generalized gradient approximation (GGA) of Perdew-Burke-Ernzerhof (PBE) functional. The Integration accuracy is set as fine, SCF tolerance is fine, and the basis set is DNP+ in Dmol3 code. The equilibrium structure has been optimized with high precision. In addition, Spin polarizations was considered in all calculations. Finally, adsorbed energies of molecule were calculated as by: $E_b=E(1+nA)-E_1-nE(A)$. Where E(1+nA) is the energy of polymer with anion A (Cl and $[ZnCl_4]$), the E1 is the energy of polymer and E(A) is the energy of A, n is the number of A.

The electrochemical measurements of Polypyrene||Zinc batteries: The working electrode was

prepared by mixing polypyrene, ketjen black, and polyvinylidene fluoride (PVDF) (5: 3 :2 by mass) in N-methylpyrrolidinone (NMP) and the resulting slurry was coated on a carbon-fiber paper current collector before drying at 80 ^{o}C for 12 h in a vacuum oven. The active mass loading is around 1.5 mg cm^{-2}. The cyclic voltammetry measurement was conducted in three-electrode cells using the polymers as cathodes, Zn metal as both the reference and counter electrodes, and $ZnCl_2$ aqueous solution as the electrolyte. The galvanostatic charge/discharge performance of polypyrene was evaluated in two-electrode cells by using polypyrene as working electrode, Zn foil as both the reference and counter electrodes, and glass fiber membrane as the separator in $ZnCl_2$ electrolyte with different concentrations. The cyclic voltammetry curves were run on a Gamry Interface 1010E workstation. The galvanostatic charge/discharge measurements were studied on an LANHE CT2001A battery tester.

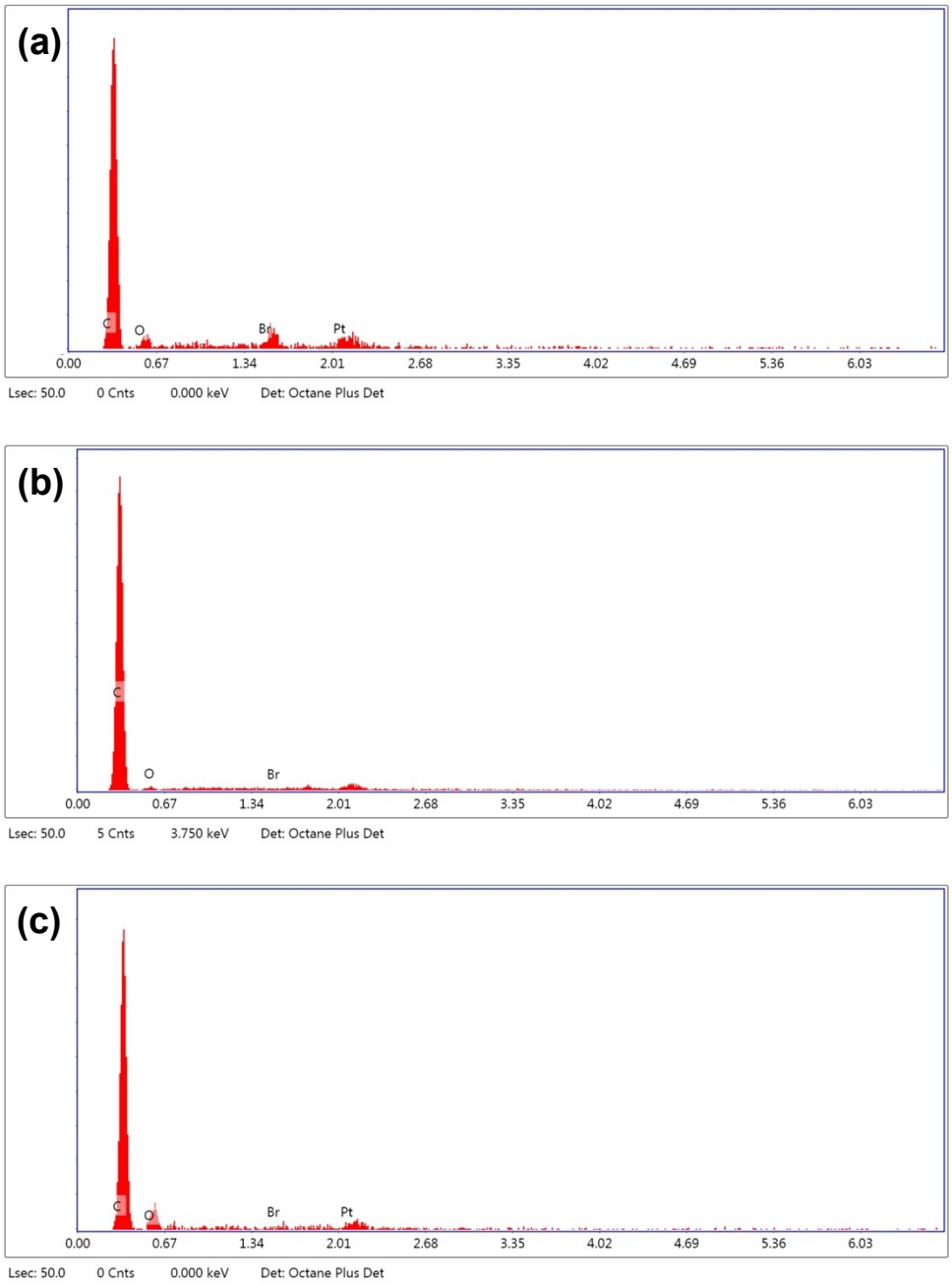

Fig. S1 The EDX spectra of (a) LPy-1, (b) LPy-2 and (c) CLPy.

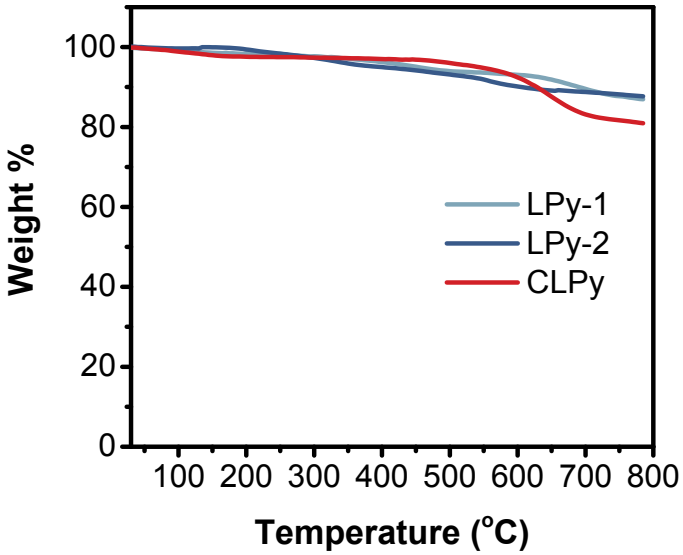

Fig. S2 The TGA curves of LPy-1, LPy-2 and CLPy under a N_2 atmosphere.

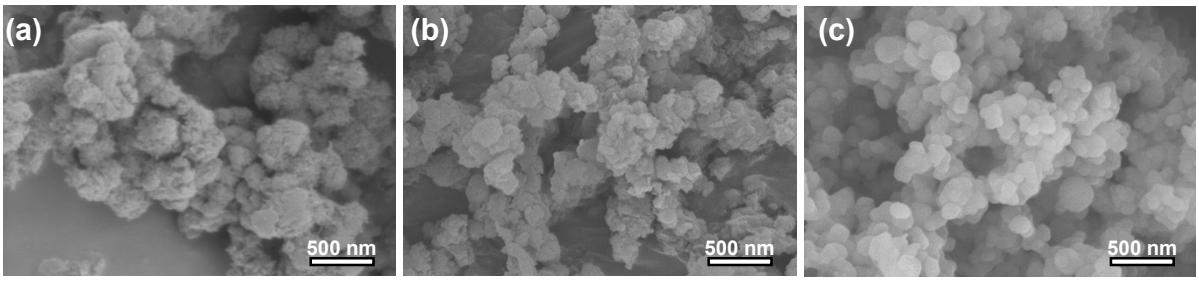

Fig. S3 The SEM images of (a) LPy-1, (b) LPy-2 and (c) CLPy.

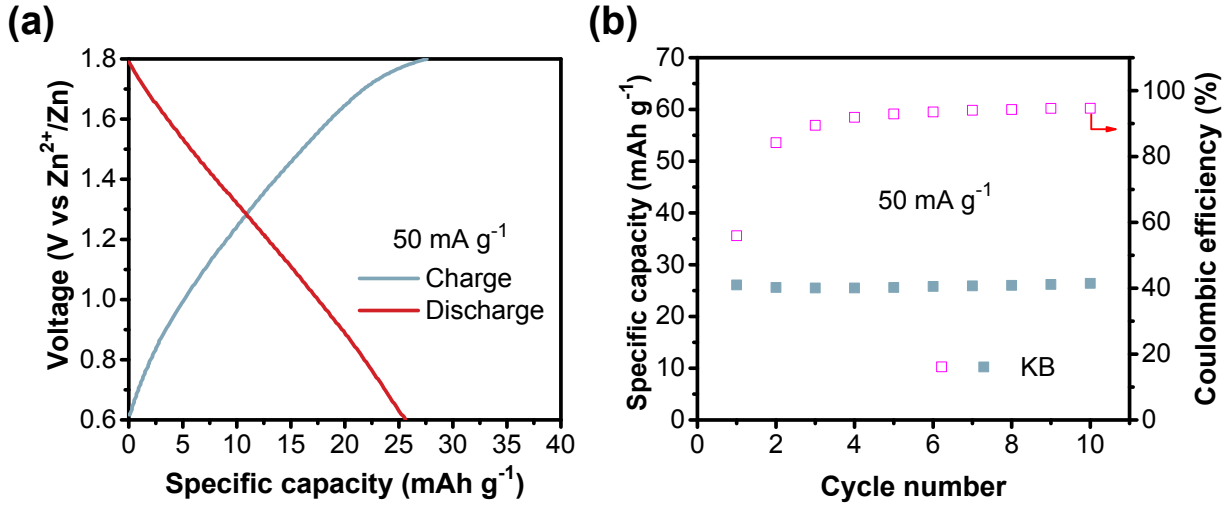

Fig. S4 The (a) GCD curves and (b) cycling performance of conductive additive Ketjen black at room temperature.

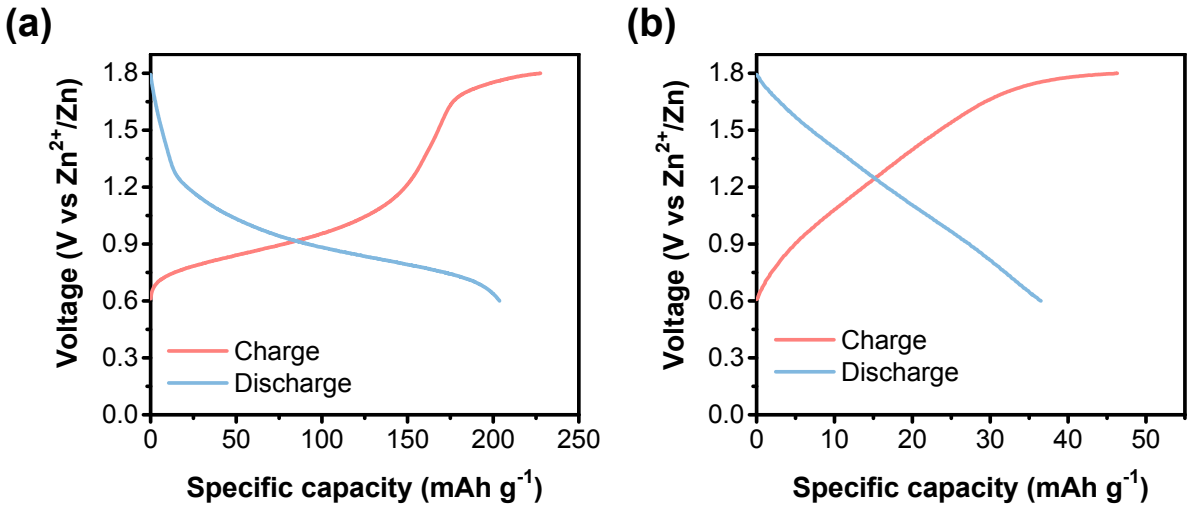

Fig. S5 The GCD profiles of (a) CLPy and (b) Ketjen black at 50 °C. The specific capacities of CLPy cathode and Ketjen black are 204 and 37 mAh g^{-1}, respectively. Therefore, the CLPy delivers a higher specific capacity of 182 mAh g^{-1} after subtracting the capacity (22.2 mAh g^{-1}) from conductive carbon additive at 50 °C. In addition, the high temperature also decreased the Coulombic efficiency of the battery due to the increased side reactions in the battery at a higher temperature.

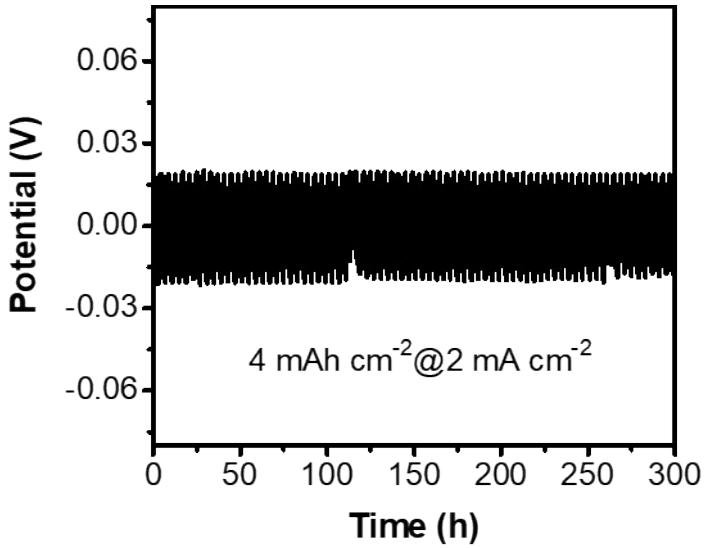

Fig. S6 The stability of Zn anode in a symmetric cell using 30 m $ZnCl_2$ as the electrolyte and Zn metal as the both electrodes at 2 mA cm^{-2} with an areal capacity of 4 mAh cm^{-2}.

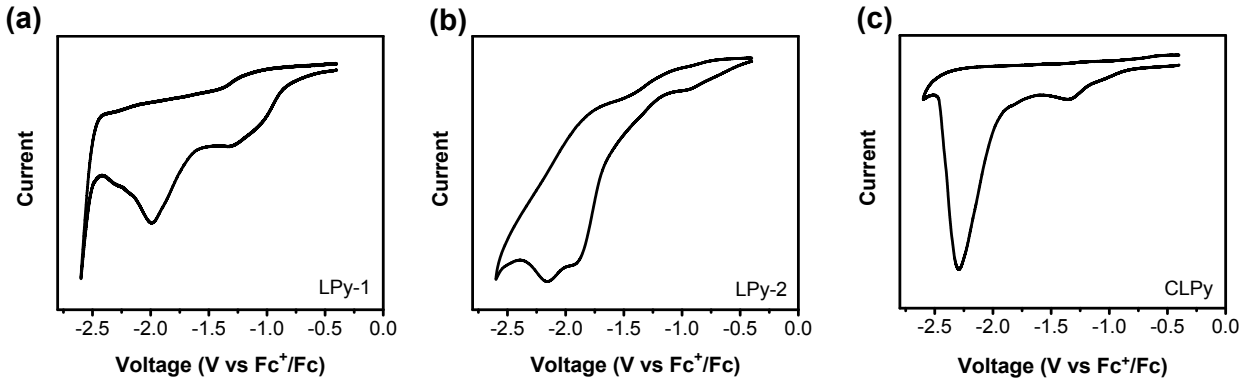

Fig. S7 Cyclic voltammogram curves for the polypyrenes at 0.1 V s^{-1}. (a) LPy-1. (b) LPy-2. (c) CLPy.

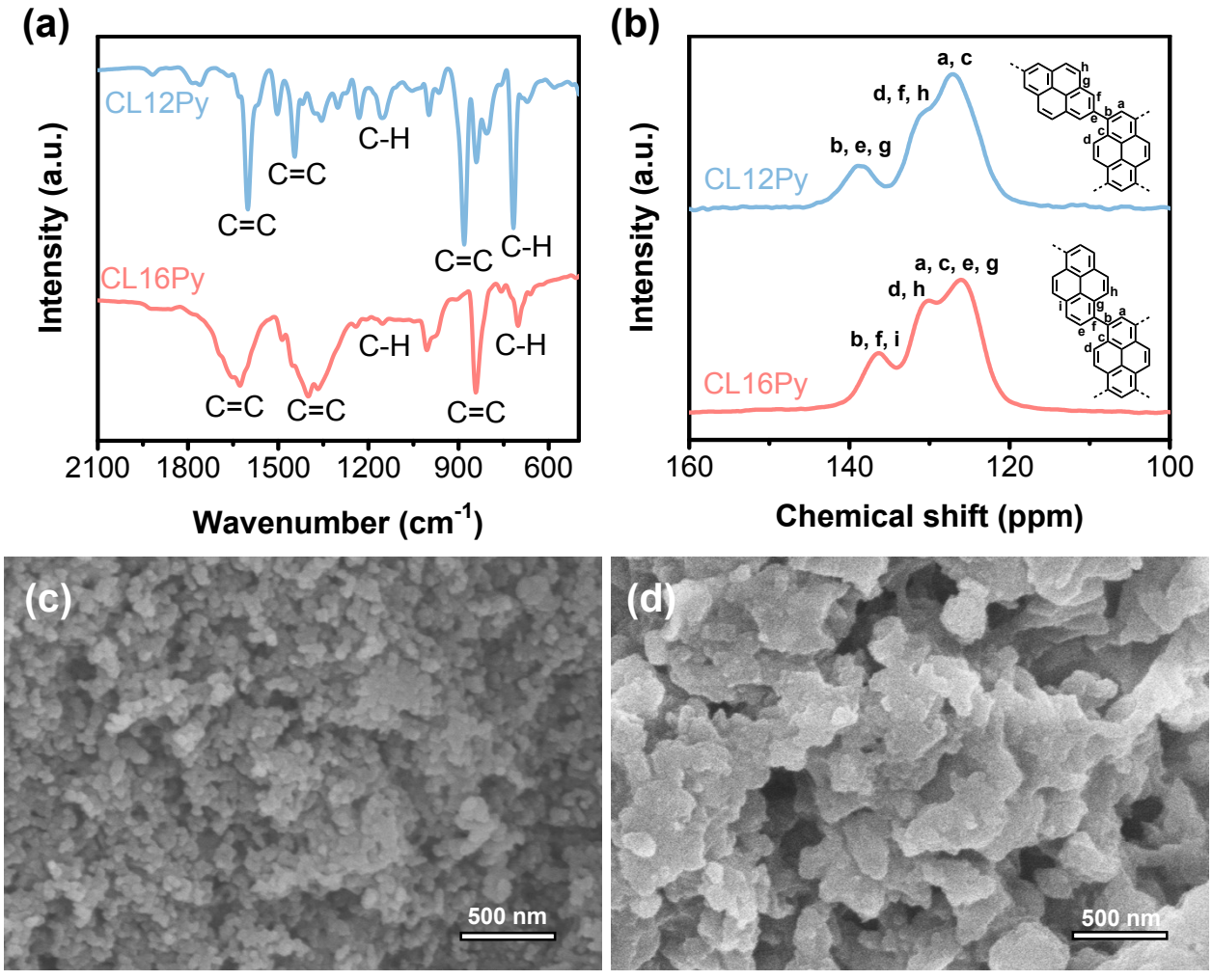

Fig. S8 The structure characterization of CL12Py and CL16Py. (a) FT-IR spectra. (b) solid state ^{13}C NMR. The SEM images of (c) CL12Py and (d) CL16Py.

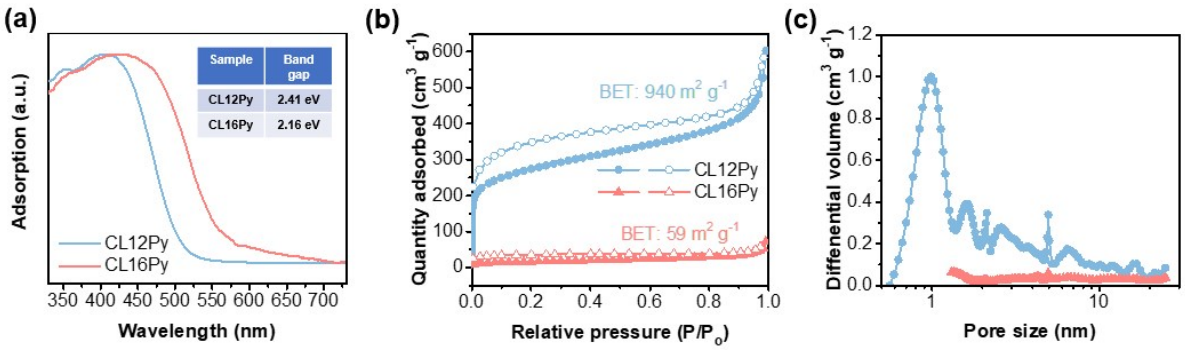

Fig. S9 The properties of CL12Py and CL16Py. (a) UV/Vis absorbance spectra. (b) N_2 adsorption-desorption curves. (c) Pore size distribution curves.

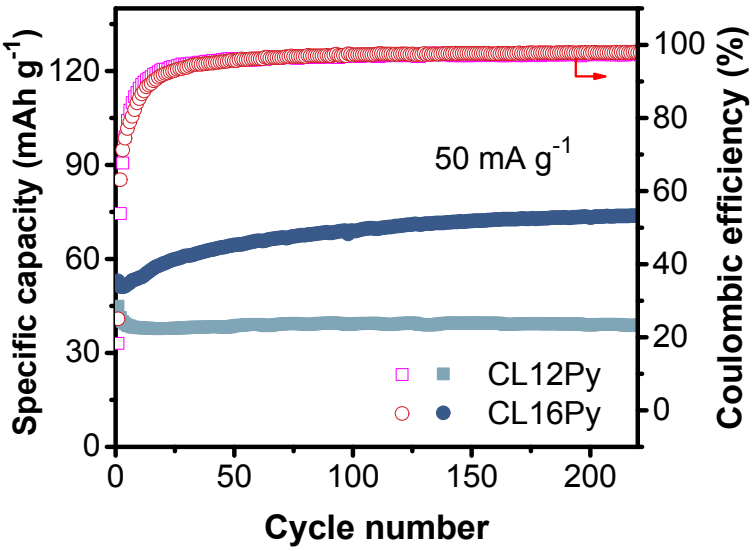

Fig. S10 The cycling performance of CL12Py and CL16Py. The specific capacity of CL16Py increased with cycling, indicating an activated process due to the continuous infiltration of the electrolyte into CL16Py, which should be attributed to its low surface area (**Fig. S9**). The highly crosslinked structure with high surface area up to 940 m^2 g^{-1} enables CL12Py to show very stable cycling performance.

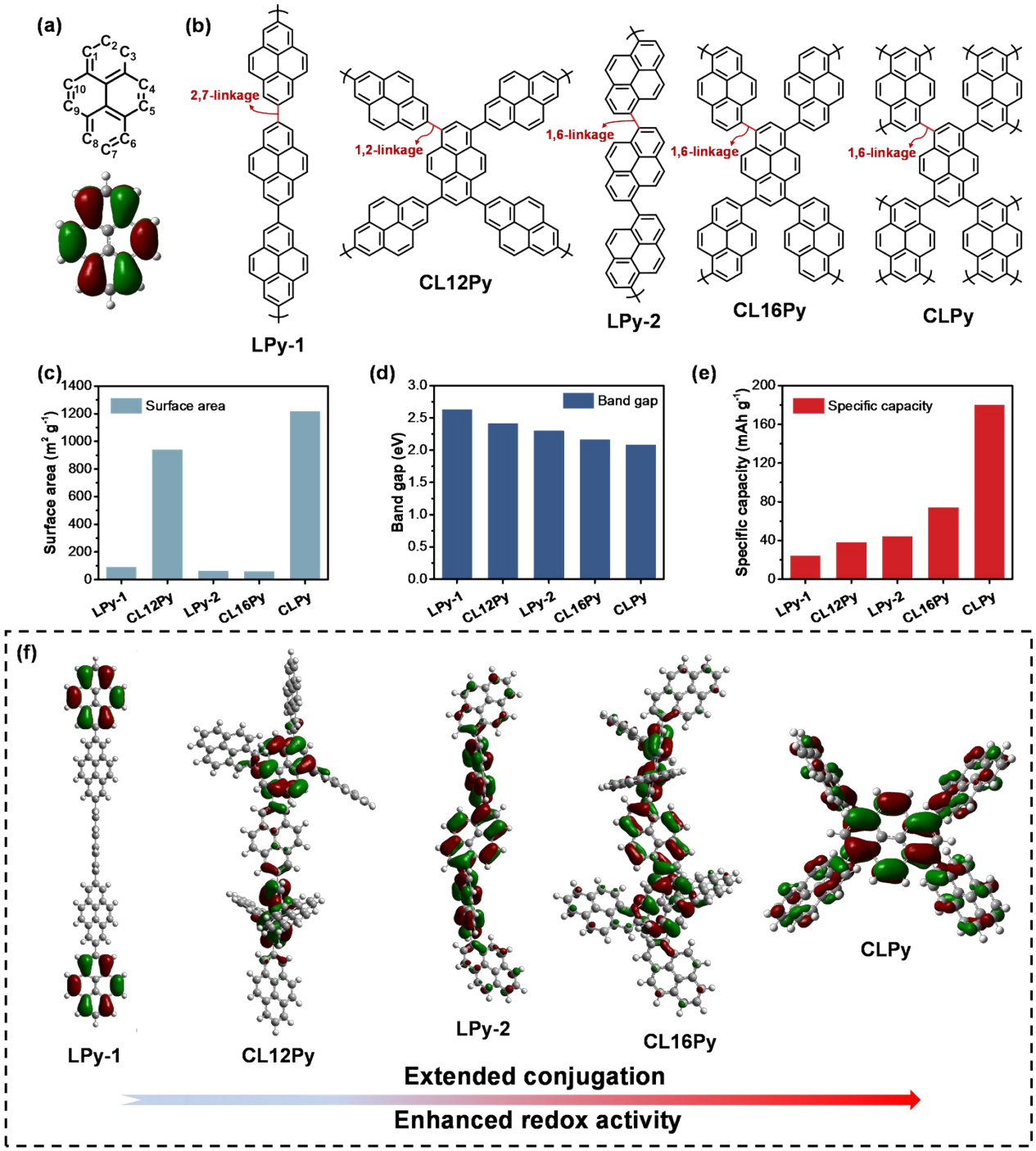

Fig. S11 The polymer structures, properties and the specific capacities for the pyrene unit and the five synthesized polypyrenes. (a) The structure with numbered carbon (top) and the HOMO diagram (bottom) for the pyrene unit. (b) The polymer structures. (c) The surface areas. (d) The band gaps. (e) The specific capacities. (f) The HOMO distribution.

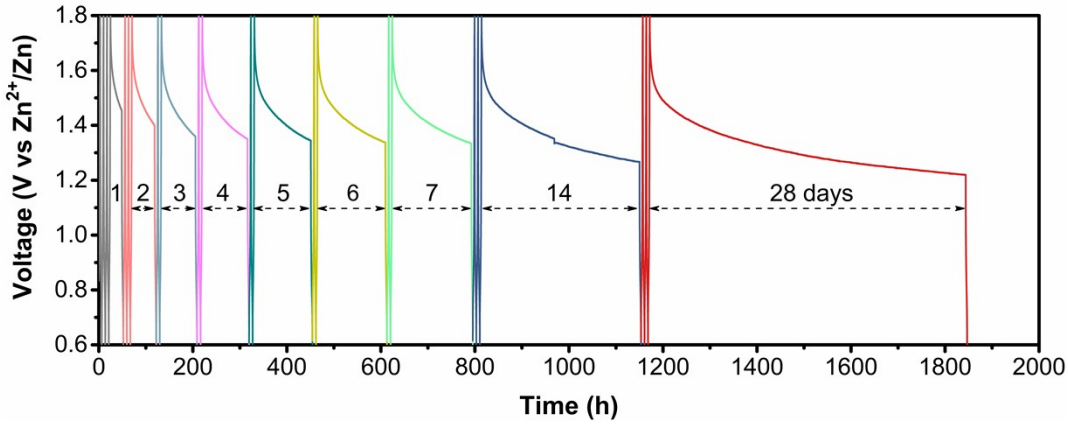

Fig. S12 The GCD curves of CLPy with different resting time.

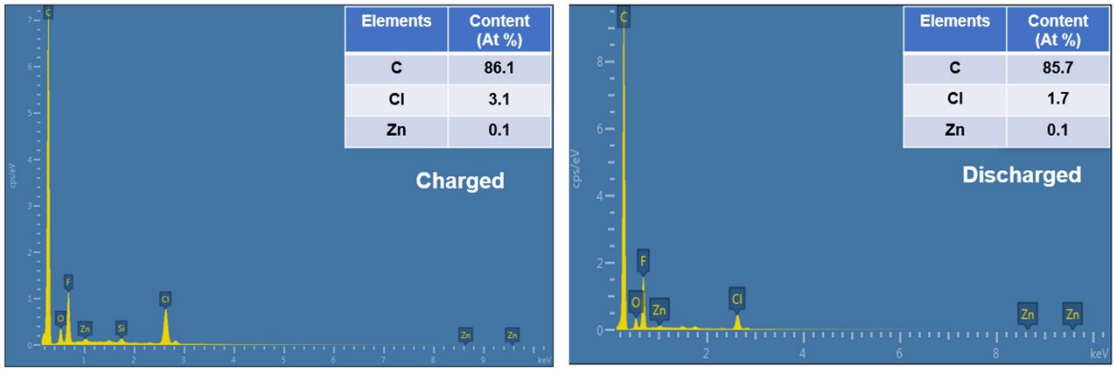

Fig. S13 The EDX data of CLPy at charged (left) and discharged (right) states.

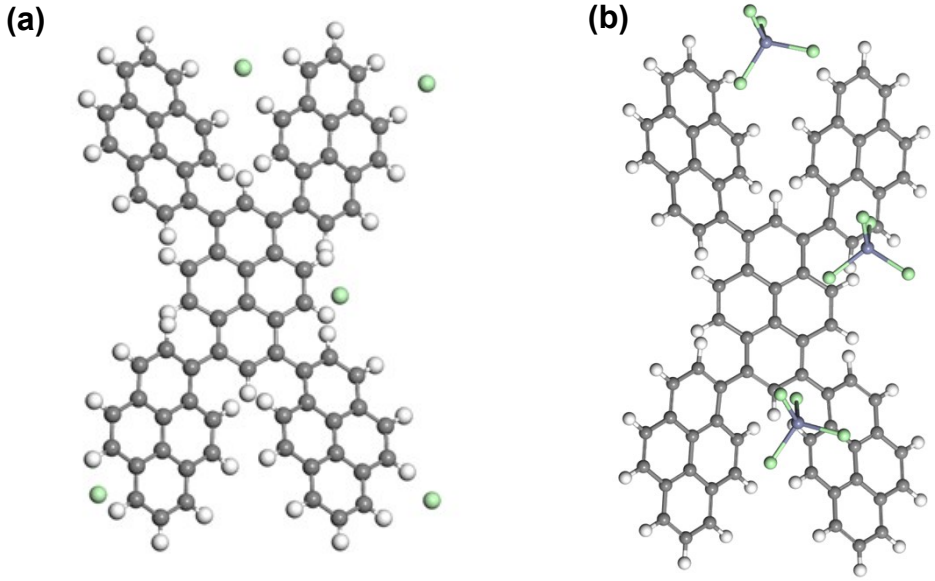

Fig. S14 The optimized structures of CLPy bound with (a) Cl^- and (b) $[ZnCl4]^{2-}$. White: hydrogen; Gray: carbon; Green: chlorine; Purple: zinc.

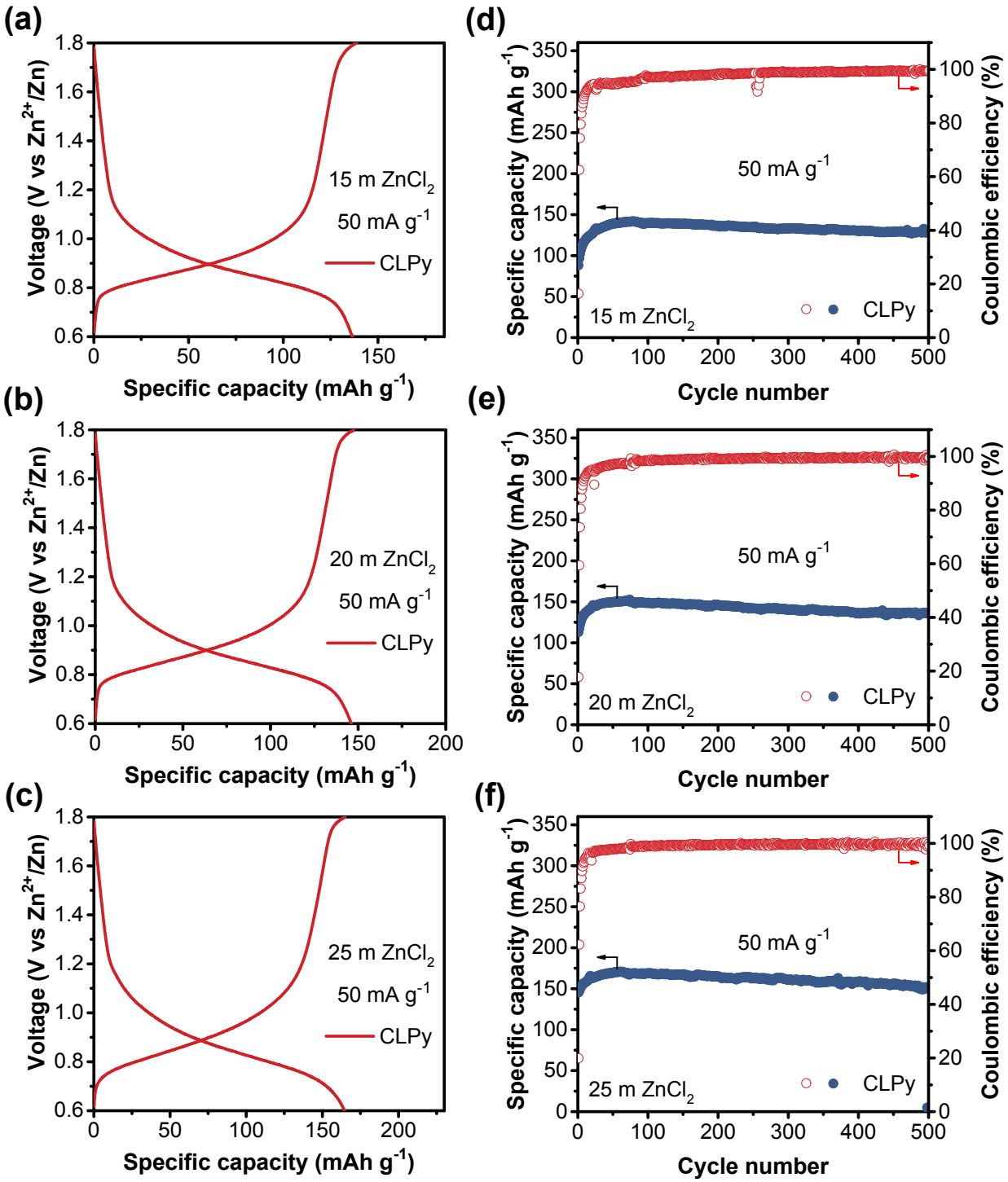

Fig. S15 The 200th GCD curves (a-c) and the cycling performance (d-f) of CLPy at 50 mA g^{-1} in aqueous $ZnCl_2$ electrolytes with different concentrations.

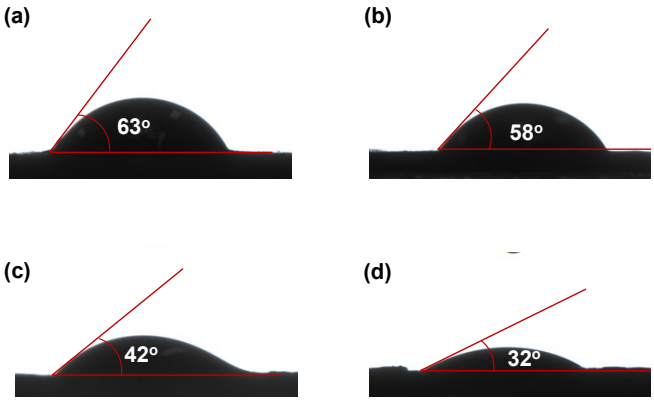

Fig. S16 The contact angle between $ZnCl_2$ solution with different concentrations and CLPy: (a) 15 m, (b) 20 m, (c) 25 m, (d) 30 m.

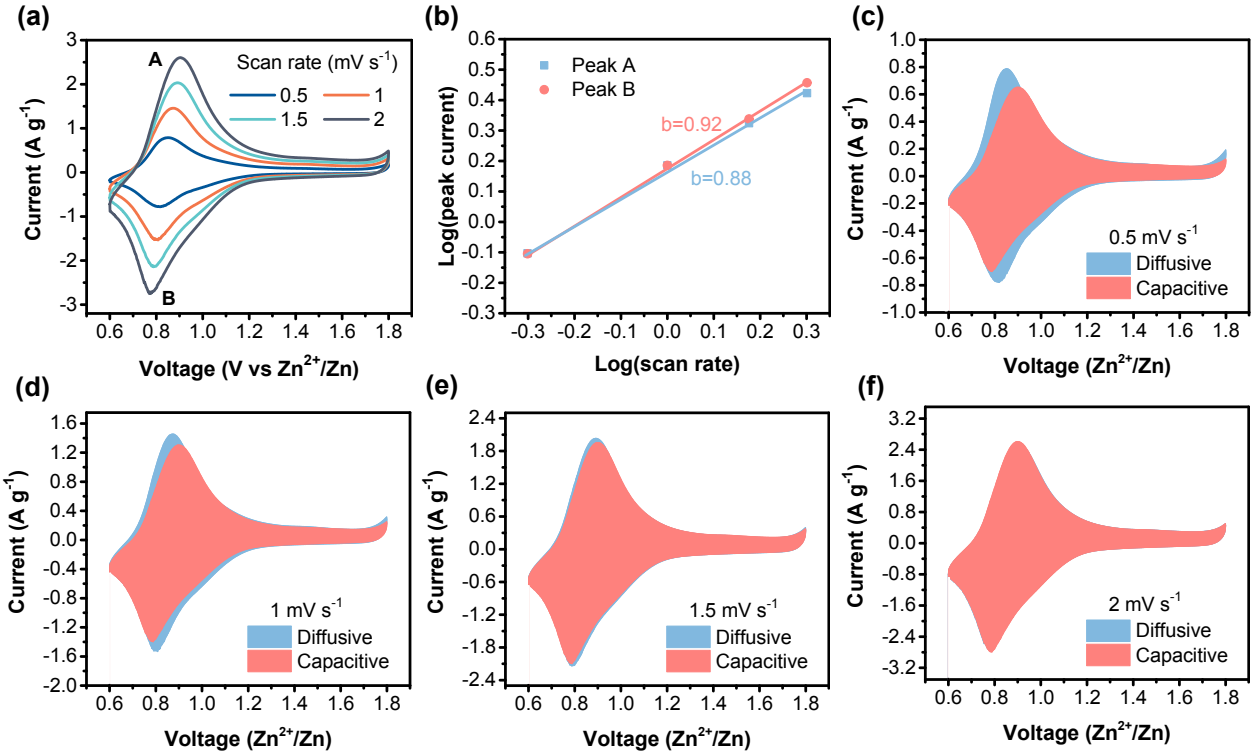

Fig. S17 (a) The CV curves of CLPy at different scan rates. (b) The fitted linear relationship between log (scan rate) and log (peak current). The capacitive contribution at (c) 0.5, (d) 1, (e) 1.5, and (f) 2 mV s^{-1}.

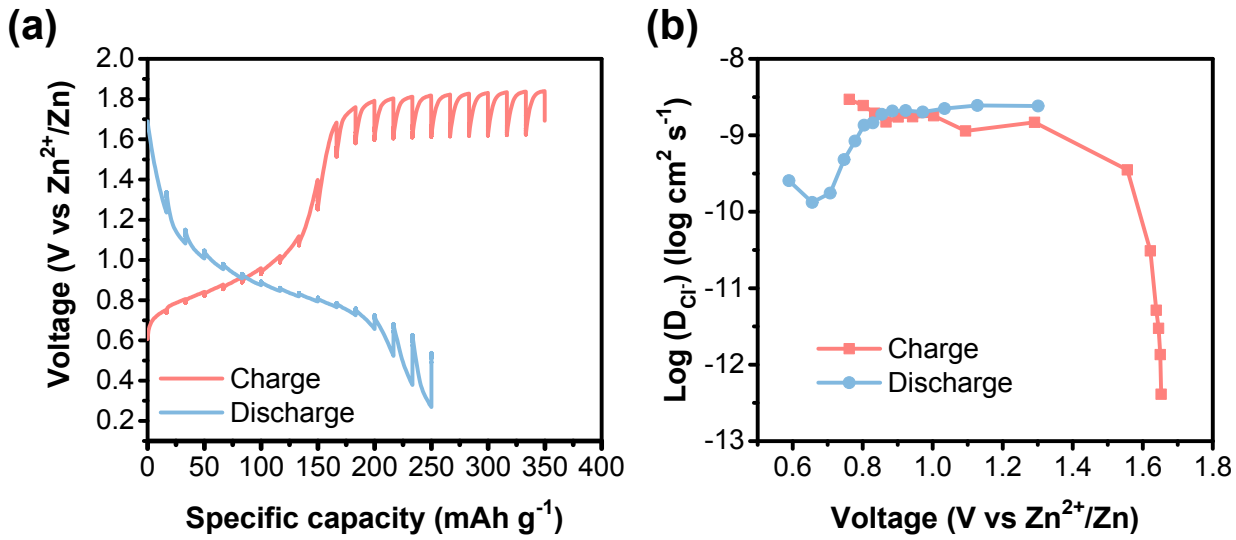

Fig. S18 (a)The GITT response for CLPy. (b) The calculated diffusivity coefficient of Cl^- at charge and discharge process.

Table S1. The comparison of electrochemical performance of CLPy with those of anion-hosting organic cathodes in recent investigations.

Sample	Electrolyte	Charge carrier	Capacity (mAh/g)	Capacity retention (cycles, current)	Ref.
CLPy	aq. 30 m $ZnCl_2$	Cl^-	180	97.4% (800, 0.05 A/g) 96.4% (38000, 3 A/g)	This work
Polyindole	aq. 1 M $ZnCl_2$	Cl^-	81	98% (200, 500 A/cm^2)	5
Poly(2-ethynyl(exTTF))	aq. 1 M $Zn(BF_4)_2$	BF_4^-	106	86% (10000, 1.06 A/g)	6
PTPAn	aq. 21 m LiTFSI	$TFSI^-$	105	86% (700, 0.5 A/g)	7
PTVE	aq. 0.1 M $ZnCl_2$ + 0.1 M NH_4Cl	Cl^-	131	65% (500, 0.5 A/g)	8
BDB	aq. 19 m LiTFSI + $Zn(OTf)_2$	$TFSI^-$, OTf^-	125	82% (500, 0.39 A/g)	9
OPr	1 M $NaClO_4$ in PC	ClO_4^-	121	69% (50, 0.02 A/g)	10
FWNT/polyaminopyrene	1 M $LiPF_6$ in EC:DMC	PF_6^-	175	85% (11000, 10 A/g)	11
poly(nitropyrene-co-pyrene)	$AlCl_3$/[EMIm]Cl	$AlCl_4^-$	100	~ 80% (1000, 0.2 A/g)	12
PPYS/COFs	1 M $LiClO_4$ in PC	ClO_4^-	145	> 100% (1000, 1 A/g)	13
PVMPT	1 M $LiPF_6$ in EC:DMC	PF_6^-	56	~100% (10000, 1.12 A/g)	14
X-PVMPT	1 M $LiPF_6$ in EC:DMC	PF_6^-	112	95% (1000, 0.112 A/g)	15
P1a	1 M $LiPF_6$ in EC:DMC	PF_6^-	35	> 100% (30000, 3.6 A/g)	16
Et-PXZ/SWNT	5 M $LiClO_4$ in EC:DMC	ClO_4^-	244.2	86% (100, 0.3 A/g)	17
3PXZ/CMK-3	2 M LiTFSI in DOL/DME	$TFSI^-$	112	80% (500, 0.645 A/g)	18
Perylene	1 M $LiPF_6$ in EC:DEC	PF_6^-	~90	~50% (1800, 0.02 A/g)	19
P1	1 M KPF_6 in DMC	PF_6^-	~170	~68% (1500, 10 A/g)	20
PDPPD	1 M $LiPF_6$ in EC:DMC	PF_6^-	102	67% (5000, 20.9 A/g)	21
P3	1 M $LiClO_4$ in EC:DMC	ClO_4^-	133	85% (200, 0.204 A/g)	22

References

1 S. Sasaki, S. Suzuki, K. Igawa, K. Morokuma and G.-i. Konishi, *J. Org. Chem.*, 2017, **82**, 6865-6873.

2 J.-H. Kim, S. Lee, I.-N. Kang, M.-J. Park and D.-H. Hwang, *J. Polym. Sci., Part A: Polym. Chem.*, 2012, **50**, 3415-3424.

3 G. Venkataramana and S. Sankararaman, *Eur. J. Org. Chem.*, 2005, **2005**, 4162-4166.

4 R. S. Sprick, J.-X. Jiang, B. Bonillo, S. Ren, T. Ratvijitvech, P. Guiglion, M. A. Zwijnenburg, D. J. Adams and A. I. Cooper, *J. Am. Chem. Soc.*, 2015, **137**, 3265-3270.

5 C. Zhijiang and H. Chengwei, *J. Power Sources*, 2011, **196**, 10731-10736.

6 B. Häupler, C. Rössel, A. M. Schwenke, J. Winsberg, D. Schmidt, A. Wild and U. S. Schubert, *NPG Asia Mater.*, 2016, **8**, e283-e283.

7 X. Dong, H. Yu, Y. Ma, J. L. Bao, D. G. Truhlar, Y. Wang and Y. Xia, *Chem. Eur. J.*, 2017, **23**, 2560-2565.

8 K. Koshika, N. Sano, K. Oyaizu and H. Nishide, *Macromol. Chem. Phys.*, 2009, **210**, 1989-1995.

9 H. Glatz, E. Lizundia, F. Pacifico and D. Kundu, *ACS Appl. Energy Mater.*, 2019, **2**, 1288-1294.

10 S. C. Han, E. G. Bae, H. Lim and M. Pyo, *J. Power Sources*, 2014, **254**, 73-79.

11 J. C. Bachman, R. Kavian, D. J. Graham, D. Y. Kim, S. Noda, D. G. Nocera, Y. Shao-Horn and S. W. Lee, *Nat. Commun.*, 2015, **6**, 7040.

12 M. Walter, K. V. Kravchyk, C. Böfer, R. Widmer and M. V. Kovalenko, *Adv. Mater.*, 2018, **30**, 1705644.

13 M. Tang, C. Jiang, S. Liu, X. Li, Y. Chen, Y. Wu, J. Ma and C. Wang, *Energy Storage Mater.*, 2020, **27**, 35-42.

14 M. Kolek, F. Otteny, P. Schmidt, C. Mück-Lichtenfeld, C. Einholz, J. Becking, E. Schleicher, M. Winter, P. Bieker and B. Esser, *Energy Environ. Sci.*, 2017, **10**, 2334-2341.

15 F. Otteny, M. Kolek, J. Becking, M. Winter, P. Bieker and B. Esser, *Adv. Energy Mater.*, 2018, **8**, 1802151.

16 P. Acker, L. Rzesny, C. F. N. Marchiori, C. M. Araujo and B. Esser, *Adv. Funct. Mater.*, 2019, **29**, 1906436.

17 S. Lee, K. Lee, K. Ku, J. Hong, S. Y. Park, J. E. Kwon and K. Kang, *Adv. Energy Mater.*, 2020, **10**, 2001635.

18 K. Lee, I. E. Serdiuk, G. Kwon, D. J. Min, K. Kang, S. Y. Park and J. E. Kwon, *Energy Environ. Sci.*, 2020, 10.1039/D0EE01003K.

19 I. A. Rodríguez-Pérez, C. Bommier, D. D. Fuller, D. P. Leonard, A. G. Williams and X. Ji, *ACS Appl. Mater. Interfaces*, 2018, **10**, 43311-43315.

20 R. R. Kapaev, F. A. Obrezkov, K. J. Stevenson and P. A. Troshin, *Chem. Commun.*, 2019, **55**, 11758-11761.

21 F. A. Obrezkov, A. F. Shestakov, V. F. Traven, K. J. Stevenson and P. A. Troshin, *J. Mater. Chem. A*, 2019, **7**, 11430-11437.

22 P. Acker, M. E. Speer, J. S. Wössner and B. Esser, *J. Mater. Chem. A*, 2020, **8**, 11195-11201.